Article:

eprints@whiterose.ac.uk
https://eprints.whiterose.ac.uk/

Loss performance of an additively manufactured axial flux machine stator with an eddy-current limiting structure

Alexander D. Goodall [a],[*], FNU Nishanth [b], Eric L. Severson [b], Iain Todd [a]

[a] *Department of Materials Science and Engineering, University of Sheffield, Sheffield, UK*
[b] *Department of Electrical and Computer Engineering, University of Wisconsin-Madison, Madison, USA*

ARTICLE INFO

ABSTRACT

AC electrical machines have mostly been limited to 2D magnetic circuits due to the use of electrical-steel laminations, however, in recent years advances in non-traditional motor architectures such as axial flux show promise for increased torque and power densities. 3D magnetic circuits as required by axial flux motors are difficult to manufacture using laminations, and for other architectures impossible. Soft magnetic composites enable 3D flux pathways but at the expense of magnetic properties. In this study, an axial flux stator is fabricated from high-silicon electrical steel (Fe-6.5 wt%Si) using additive manufacturing with Hilbert cross-sectional geometry to limit eddy current losses and compared with electrical steel laminations of 0.127 mm and 0.35 mm. This shows comparable performance between the additively manufactured Hilbert stator and 0.35 mm laminations below 500 Hz. A torque loss of approximately 20% was observed due to 34% less magnetic material in the Hilbert stator than 0.127 mm laminations, but improved torque density for the stator by 13%. By designing for additive manufacturing, tooth area could be scaled up providing an electrical machine with 3D magnetic flux pathways with acceptable loss behaviour and good magnetic circuit properties, enabling further flexibility to electrical engineers in their pursuit of higher torque and power density.

1. Introduction

For decades, electrical steel laminations have been used to reduce eddy current losses in electrical machines (EMs) [1]. By limiting the generated eddy currents to a thin sheet of material the generated currents are smaller and hence losses via joule heating are also reduced. However, laminations restrict the magnetic flux circuit to two dimensions as the magnetic flux must run in the plane of the lamination. This has made 3D magnetic flux circuits rare, and when implemented alternatives such as soft magnetic composites (SMCs) are often used for the stator to reduce the core loss, especially at high frequencies [2], however, this comes at the cost of magnetic properties such as permeability. Axial flux machines have shown potential for achieving high torque density [3], however, these machines require a 3D magnetic circuit. Techniques available to manufacture the stator cores of axial flux machines and axial flux topologies are reviewed in [3]. It is possible to achieve this by using coil wound electrical steel laminations [4–6], however, any advances in this design to enable things such as magnetically levitating bearings [7,8] or more complex flux pathways will not be possible to be fabricated in this way as the radial dimensions will not

be constant. SMCs have also been used for axial flux stators [9–11], demonstrating lower core loss than electrical steel laminations at high frequencies, but again have limitations on shape due to the uniaxial pressing operation. As the capacity to create 3D magnetic circuits with acceptable loss behaviour has not yet been possible, machines using this configuration have rarely been investigated.

Further to this, high silicon electrical steel is shown to be a promising soft-magnetic material for future electrical machines [12] with a higher resistivity yielding lower core loss, however, the brittle nature of this alloy has posed difficulties with processing meaning that rolling into thin sheets is not a commercially viable option. Alternative methods such as diffusion of Si into Fe-3 wt%Si sheets have been used with some success [13], but not yet widely adopted, and as a result, Fe-3 wt%Si is more commonly used [14].

Additive manufacturing (AM) has the ability to combat both of these issues, having successfully been used to process high silicon electrical steel [15,16], near fully dense, and with good magnetic properties such as permeability up to 30,000 [17]. This is enabled by the high cooling rates of the AM process avoiding the ordered phases that cause embrittlement in the high silicon alloy. Therefore, soft magnetic

components can be processed via AM, however, the process cannot mimic the small material thickness and surface quality of electrical steel laminations, therefore alternative methods to avoid large eddy currents in bulk sections must be investigated. Cross-sectional geometries have been shown to reduce the eddy current losses such as slotted geometries similar to laminations [18–21], topologically optimised parts [22] and complex geometries such as the Hilbert pattern [23] demonstrated first by Plotkowski et al. [16]. These methods are reviewed in [24]. The Hilbert pattern used by Plotkowski et al. was built with the cross-sectional geometry being resolved perpendicular to the build platform, which is the easiest orientation to achieve high resolution in laser powder bed fusion (L-PBF), however, this restricted Plotkowski et al. from building 3D flux pathways. As such testing of these materials required a mini-Epstein frame style fixture to join together 4 legs of material to enable a magnetic circuit to be created. For characterising the losses of this geometry this is an effective method, however for AM to be useful in electrical machines it must be able to achieve continuous 3D flux pathways, otherwise electrical steel laminations are likely to outperform electrical steel produced by AM. Plotkowski et al. have also demonstrated this pattern in a real world application by building a transformer [25], however, this again has 2D flux pathways and multiple locations where the magnetic circuit is not continuous.

This study will characterise the Hilbert cross-sectional geometry when built parallel to the build platform, the most difficult orientation for this pattern due to horizontal overhung surfaces. A design rule will be established to reduce electrical shorting across areas that should not be connected. Once enabled in this direction the Hilbert cross-sectional geometry could be implemented into any orientation in the build chamber, and therefore the stator of an axial flux permanent magnet (AFPM) machine is designed and built using AM, which has 3D magnetic flux pathways. The performance of this stator is compared to that of a prototype stator built using electrical steel laminations but is not suitable for volume production.

2. Materials and methods

2.1. Additive manufacturing and heat treatment

All AM samples were manufactured using L-PBF. AM of toroidal ring samples for magnetic characterisation and samples for determining minimum gap sizes were built using an AconityMINI from Aconity3D GmbH with a build platform of 140 mm diameter. This machine uses a 200 ytterbium-doped continuous laser with a spot size of 70 μm. The AM Hilbert stator was manufactured using an AconityLAB from Aconity3D GmbH, with a larger build platform of 170 mm diameter, equipped with a 400 W ytterbium-doped continuous laser with a spot size of 70 μm. The vertical direction normal to the build platform, also known as the build direction is referred to throughout this work as the Z axis, whereas the orthogonal directions parallel to the build platform are referred to as X and Y.

All samples were built using high silicon electrical steel powder (Fe-6.5 wt%Si) supplied by Höganäs AB, with a powder size of 15–45 μm. The layer thickness was kept constant at 30 μm, with a 67° layer rotation. The process is completed under an argon atmosphere, with oxygen content kept below 400 ppm. All samples were built onto stainless steel baseplates. Laser power and laser speed were kept constant at 170 W and 0.7 m/s respectively. Wire electrode discharge machining (EDM) is used to remove all samples from the build platform. All samples are removed before heat treatment except for the AM Hilbert stator, which was removed after heat treatment.

All samples were designed using Creo 8 provided by PTC. After exporting to.STL files, Netfabb premium 2021 (Autodesk) was used to arrange parts on the build platform and assign parameters, before creating.ILT files which can be used directly by the Aconity machines. Hatch offset and fill offset were 0.1 mm and 0.15 mm respectively, with a hatch spacing of 70 μm.

Heat treatment was done in-house using a tube furnace for the toroidal ring samples and externally by MSL heat treatment LTD for the AM Hilbert stator. All heat treatments used a heating rate of 5 °C per minute, then held at a temperature of 1150 °C for 1 h, followed by furnace cooling, as demonstrated by Garibaldi et al. [26]. All heat treatments were completed in an argon atmosphere.

2.2. Metallographic preparation and microscopy

Samples were cross-sectioned using a Secotom 50 (Struers), then hot mounted using a Simplimet mounting press (Buehler). Grinding and polishing were completed using a Tegramin 20 (Struers) with several steps which were; Grinding using P1200 grit paper, grinding using P2400 grit paper, polishing using 9 μm diamond suspension, polishing using 1 μm diamond suspension, polishing using 0.25 μm diamond suspension and finally polishing using Masterpolish, all supplied by Buehler.

Optical microscopy was captured using an Olympus BX51 microscope in conjunction with the Clemex Vision PE system, using a 50x magnification lens. Measurements for gaps were taken directly from the micrographs in the Clemex software.

2.3. Magnetic characterisation – ring samples

Toroidal ring samples were used to characterise the material using an AMH-1K permeameter by Laboratorio Elettrofisico. These samples had a rectangular cross-sectional area of approximately 4 × 4 mm, however, this was measured accurately for each sample. The toroid had an outer diameter of 38 mm, hence the samples respect the dimensions in BS 60404–6:2018 [27]. Samples were wound with a search coil using 0.35 mm diameter, single core copper wire with 45 turns, and a driving coil of 40 turns using 1.5 mm diameter multi-strand copper wire with PVC insulation. BH loops were measured at several frequencies from 5 Hz to 1000 Hz, which is the maximum the machine can provide, allowing for the core loss to be measured. For each toroid, a secondary sample of only ¼ of a ring was built, sectioned, and imaged to provide a stacking factor, defined as the percentage area of magnetic material / the total area including air gaps. This stacking factor was implemented into the measurements in the Neon software (Laboratorio Elettrofisico), used to control the permeameter in order to take account of the air gaps within the material.

2.4. FEA simulations and lamination loss calculations

The stator of the axial flux machine designed and optimized in [28] was selected for prototyping using AM. Two electrical steel laminates of thickness 0.127 mm and 0.35 mm were considered for comparison with the AM stator. The B-H data and the loss coefficient terms in the Steinmetz equation (Eq. 1) for the 0.127 mm and 0.35 mm laminations were obtained from the library material models from the manufacturer in Simcenter MAGNET [29]. The material model used for the 0.127 mm lamination was that of Arnon 5, while the model of M-19 29Ga was used for the 0.35 mm lamination. Two sets of 3D transient electromagnetic simulations were performed to compute the stator iron losses by assigning i) the 0.127 mm steel material and ii) the 0.35 mm steel material for the stator core. The 3D FEA model is shown in Fig. 1. The rotor yoke and permanent magnets were set up as a motion component and configured to the rated speed. Sinusoidal 3 phase current excitation, with a peak value of 140 A (rated current) was applied to the stator windings. The frequency of the current excitation was 800 Hz for the rated speed. A fixed time step of 1/20th of the fundamental time period (1.25 ms) was used for the transient FEA. Full details of the FEA model can be found in [28].
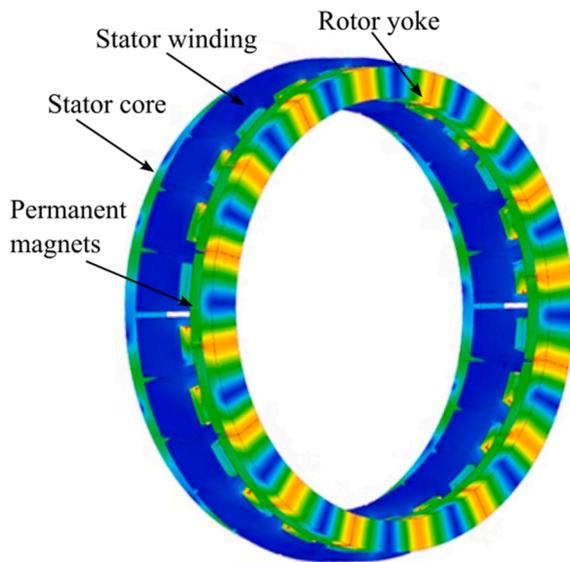
Fig. 1. 3D FEA model showing stator, rotor, permanent magnets and stator windings.

2.5. Stator winding and testing

The laminated stator was fabricated by machining slots into a tape wound core. A strip of 0.127 mm thick laminations was wound into a ring-shaped core with the same dimensions as the stator of the electric machine. The tape wound core was then bonded using an inorganic insulating adhesive to improve structural strength and prevent the layers from splaying. Next, slots were machined into the tape wound core. Finally, a layer of insulating material was coated on the machined stator core.

Rectangular 12AWG equivalent copper wire was used to make the stator coils for the conventional and additive stators to achieve high copper fill factors. Each coil had 7 turns and the stator had 24 coils. The finished stator was glued to an aluminium baseplate using a structural adhesive.

A CNC mill configured as a contact-free dynamometer was used to characterize the conventional and additive stators. A 16-pole rotor was mounted in the spindle collet while the stator was mounted on a 6-axis load cell fixed to the mill bed. The load cell was used to measure the axial forces and the reaction torque on the stator. Static torque measurement tests described in [28] were performed at different stator currents up to the rated current to validate the torque capability of the machine.

To compare the iron losses, a no-load test was performed. The stator terminals were open-circuited, and the rotor was rotated at different speeds up to 6000 RPM (corresponds to an electrical frequency of 800 Hz), using the mill spindle speed control function. The reaction torque on the stator was measured using the load cell at each speed. The product of the reaction torque T in Nm on the stator and the speed ω in rad/s was computed to obtain the stator iron losses $P_{stator} = T\omega$.

3. Results

3.1. Loss performance of Hilbert-shaped magnetic circuit

The Hilbert space-filling curve pattern has been shown to be effective at managing eddy current losses in additively manufactured Fe-Si [16, 25]. These have always been built with the cross-sectional geometry being resolved in the XY plane of the L-PBF machine. The major advantage of using AM to build soft-magnetic material is to enable 3D flux pathways. Restraining the cross-sectional geometry to one plane

also limits the magnetic circuit to a 2D path, therefore in this study, the Hilbert cross-section is built in the XZ plane, as this will be the most difficult to successfully resolve the intended geometry due to burn through of horizontal gaps from the layers above. To find out the minimum-sized gap in the XY plane a test sample was made with nominal gaps ranging from 50 to 500 μm, showing that in this plane a 50 μm gap was successfully maintained (Fig. 2a). Demonstrating this on a 4 × 4 mm cross-section, it is shown that this cross-sectional geometry will resolve correctly in the XY plane (Fig. 2b), with gaps this small, but when attempted in the XZ plane the horizontal gaps suffer from burn through, rendering the geometry unrecognisable (Fig. 2c).

The minimum gap in the XZ direction was found to be 250 μm, hence we can create a design rule for the minimum permissible gap to allow for air gaps to be maintained. The gap will differ depending on the angle of the surface being built, as shown in Fig. 2d, where the required gap to allow for 250 μm between surfaces in the Z direction is dependent on the cosine angle of the surface. This is plotted graphically in Fig. 2e demonstrating a sinusoidal reduction in the gap from horizontal surfaces (build angle 0°), to a minimum of 50 μm at approximately 80° which is then maintained until 90°.

This experiment was completed using constant laser parameters. It is possible that the parameters of the down facing surfaces may be optimised for a lower roughness, meaning that a gap smaller than 250 μm could be obtained. For these soft-magnetic material structures, it is very important to have complete isolation between the surfaces. As additive manufacturing is inherently stochastic at the scale of surface roughness, due to differences in powder spreading, powder quality, laser interaction with the powder bed, and thermal conditions, there could be some events causing short-circuiting between areas that should be electrically isolated.

The nominal gap in the CAD design is not the only factor affecting this gap, other factors such as hatch spacing, melt pool width, surface roughness, and hatch offset (distance from the edge of the CAD model to laser hatch line) can all have an impact on this gap. By using constant laser parameters during this study these parameters were kept uniform, however when transferring between different machines or software it is important to control all of these parameters.

Toroidal ring samples which used a Hilbert space filling curve based cross-sectional geometry were built with the cross-sectional pattern in the XZ plane in order to test the magnetic properties. BH loops were measured at a variety of frequencies from 5 Hz up to 1 kHz, which was the maximum permissible by the testing equipment used. Measurements were taken manipulating the magnetic field, H, until a flux density of 1 T was measured in the sample. BH loops for ideal soft-magnetic materials are demonstrated by a high initial gradient, and hence relative permeability (μ_r), followed by the knee point occurring at a high flux density, giving a higher flux density for a given magnetic field (H). Other desirable features are high magnetic saturation, low core losses represented by the area inside the loop, and low coercive force (H_c). Samples were tested in the as-built condition, then heat-treated at 1150 °C for 1 h using the procedure from Garibaldi et al. [26] and characterized again. Resulting BH loops are shown in Fig. 3, demonstrating a reducing permeability and increasing core losses with an increase in frequency. In the heat treated condition at 50 Hz and 1 T the coercive force (H_c) is 250 A/m and the maximum relative permeability is approximately 6000.

Heat treatment of the samples yields an improvement in magnetic properties, especially permeability as the BH loops have a steeper gradient prior to the knee point, which is also evidently higher. At higher frequencies such as 1 kHz, there is less difference in the BH loop shape as the eddy currents start to dominate the loss behaviour due to proportionality with the square of the frequency. This behaviour is more heavily dependent on the shape of the samples rather than the microstructural properties and therefore to be expected. Even in the heat-treated samples, the knee point is lower than would be expected from Fe-Si, where it would normally occur at approximately 1.5 T.
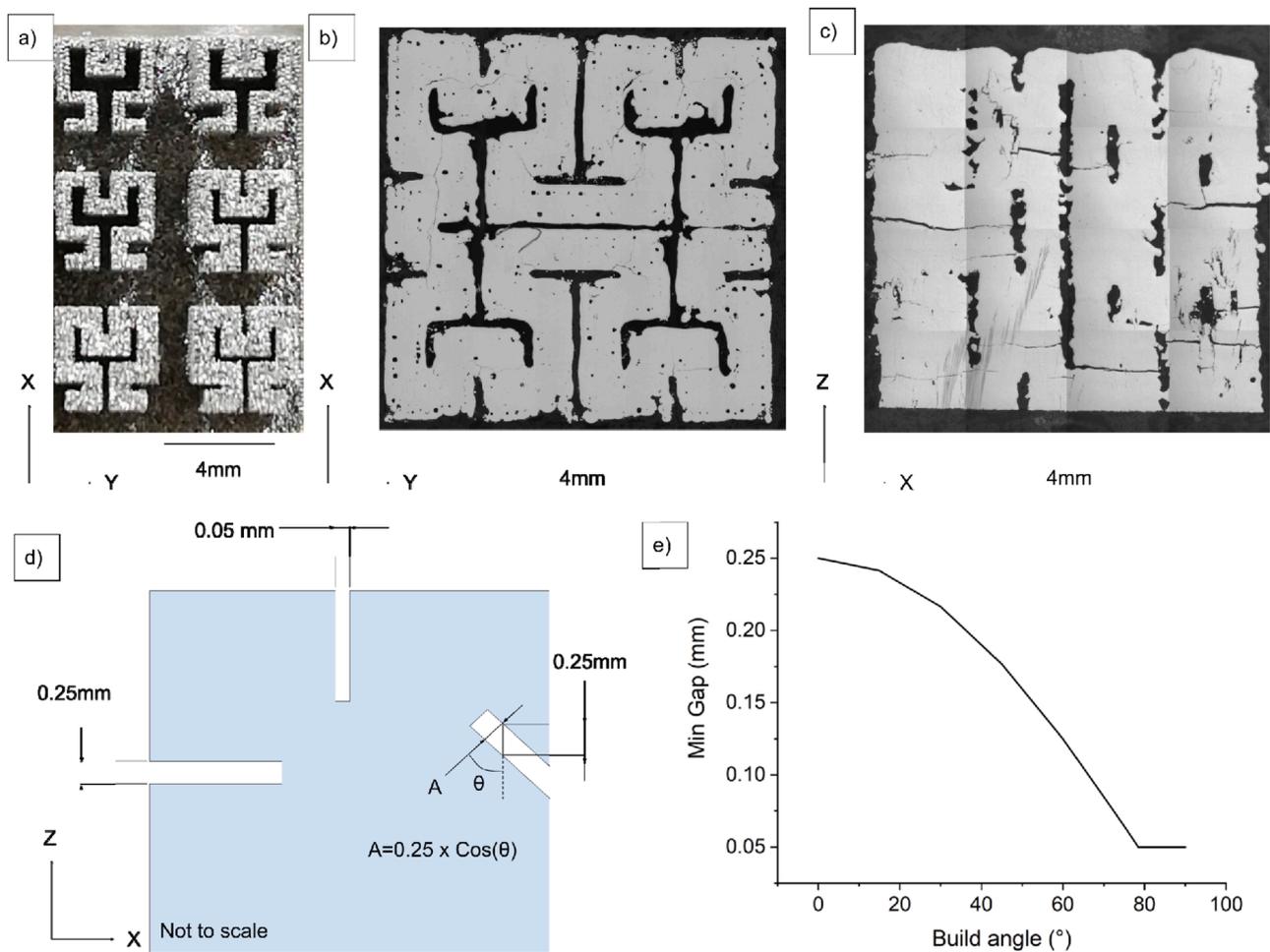
Fig. 2. Hilbert shape filling curve used to manage eddy currents, showing a test to check for the minimum sized gap in the XY plane (a), the resultant Hilbert cross-sectional geometry when the pattern is built in the XY plane (b) and XZ plane (c), along with the schematic showing the minimum gap design rule (d) and the graphical representation of the minimum gap design rule (e).
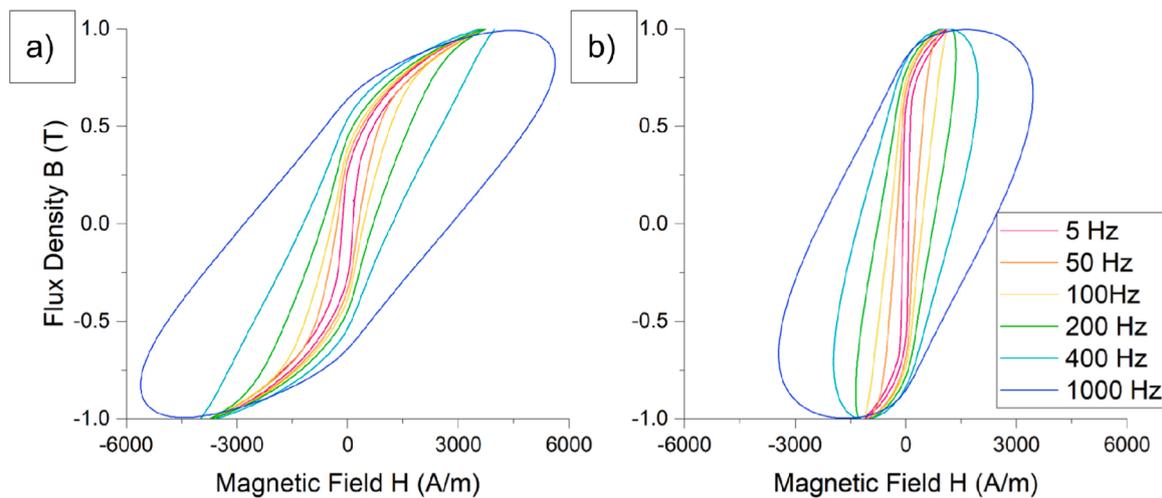
Fig. 3. BH loops of toroid samples with Hilbert cross-sectional geometry, for the as-built state (a) and heat-treated state (b). BH loops were measured at several frequencies 5–1000 Hz at a flux density of 1 T.

The core losses are plotted in Fig. 4 showing a small improvement in loss behaviour with heat treatment for the additively manufactured Hilbert samples, with core losses at 1 kHz being 1727 W/kg and 1065 W/kg for the as-built and heat-treated samples respectively. These

are plotted against core losses calculated using the Steinmetz equation [30] for electrical steel laminations of 0.127 mm and 0.35 mm. The Steinmetz equation is shown in Eq. (1), where P is the total core loss, K_h and K_e are the hysteresis and eddy current loss coefficients respectively, f
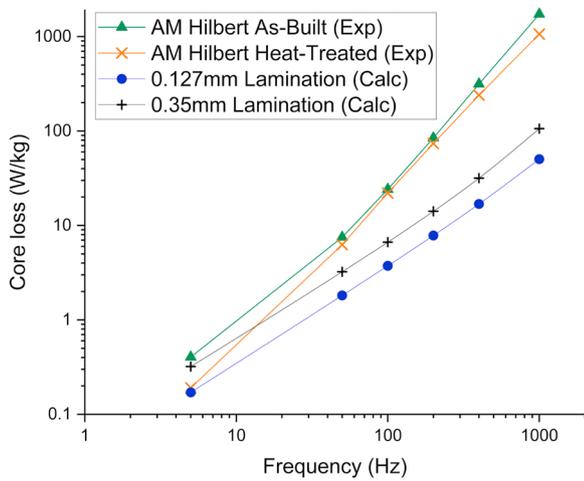
Fig. 4. Experimentally measured loss behaviour of the Hilbert ring manufactured by AM, in the as-built and heat-treated conditions, compared with data calculated for two thicknesses of laminations.

is the frequency, B is the flux density and α and β are constants.

The core losses at frequencies of 50 Hz and above are lower in electrical steel laminations than those in the additively manufactured Hilbert samples, owing to their lower wall thicknesses that cannot be reproduced using current AM technology. Eddy current losses are increased with a larger wall thickness and the wall thickness in the Hilbert structure is nominally 0.5 mm thick. At 1 kHz the core losses for the 0.127 mm and 0.35 mm laminations are calculated at 50 W/kg and 106 W/kg respectively, an order of magnitude smaller than those from

the Hilbert samples. The trend also shows the difference increasing with frequency.

$$P = K_h f^\alpha B^\beta + K_e f^2 B^2 \tag{1}$$

3.2. Design and manufacture of electrical machine stator

Having established a design rule for the minimum gaps to give electrical isolation, the design for an electrical machine stator was created using the Hilbert cross-sectional geometry. This was developed for the axial flux permanent magnet (AFPM) motor demonstrated by Nishanth et al. [28], which was designed to use a stator consisting of ring wound electrical steel laminations, 0.127 mm thick. The stator has an outside diameter of 164.5 mm and has an axial length of 35 mm. By building the Hilbert stator using AM, it is possible to obtain a direct comparison with the electrical steel laminations used in the original design.

The design of the Hilbert stator is shown in Fig. 5. There are two main regions which are the tooth and back iron of the stator. As the majority of the flux pathway within the stator is in the tooth, this region is kept in the XY plane of the AM machine in order to obtain the smallest possible air gaps within the cross-section. This allows for a higher stacking factor, which is the volumetric ratio of magnetic material to insulation, which in this case is air. The other main region is the back iron which runs circumferentially around the bottom of the stator. This must have non-uniform air gaps as the horizontal surfaces require a gap of > 250 μm, whereas the vertical surfaces require a gap of only 50 μm.

This back iron region has an approximately square cross-sectional area therefore implementing the Hilbert space filling curve is done with relative ease (Fig. 5c). However, the tooth has a non-regular shape owing to its outer and inner surfaces falling on the outer and inner
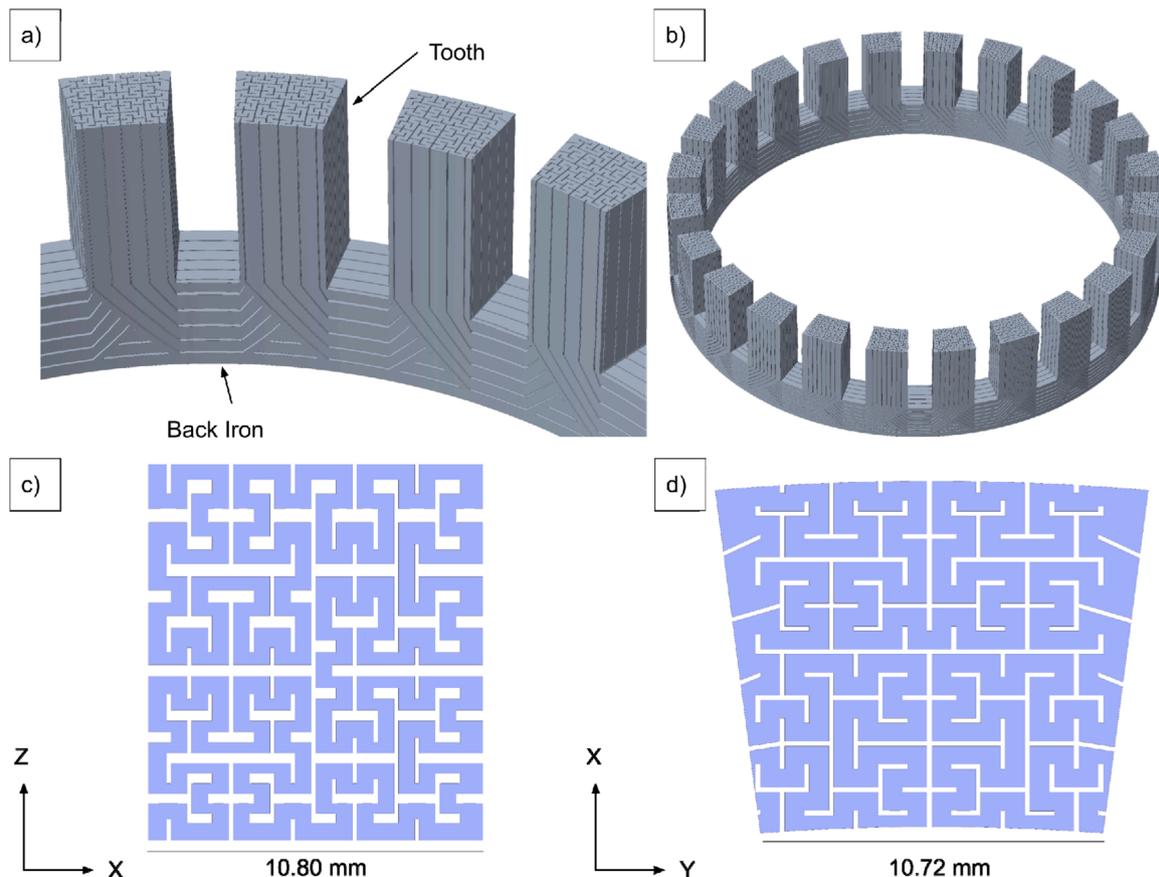
Fig. 5. Hilbert stator for AXPM machine designed to be manufactured using AM. The stator has a toothed region which has a uniform air gap size for the XY plane of the AM machine, with a back iron region with non-uniform air gaps showing more clearance in the Z direction than the X direction.

diameters of the stator. The central region of this is filled with the Hilbert space filling curve, whilst the edges are modified in a way so as to keep the intent of the shape, whilst attempting to reduce any large cross-sectional areas of bulk material (Fig. 5d). The flux pathways in this stator are axially along the tooth and circumferentially around the back iron, hence this is the direction the Hilbert cross-section is implemented. In the region where the tooth and back iron meet, the flux may run in several directions, either skipping the tooth and running circumferentially, or by leaving the tooth and running through the back iron in either direction. Due to this, the magnetic flux can be running in one of three directions in the region underneath the tooth. Therefore, the Hilbert cross-section has been implemented in these three directions. Where the flux pathways interfere with each other a simple rule was used to implement solid material or air gap. In any location, if at least one of the flux pathways' Hilbert cross-sectional pattern required solid material, then solid material is selected. The outcome of this is that in some areas where there is supposed to be an air gap, this air gap is filled with solid material from the cross-section of a different flux pathway. The full stator is shown in Fig. 5b.

This stator was designed in 3 days and successfully built in approximately 80 h. The stator was then heat-treated at 1150 °C for 1 h, to relieve residual stress, drive recrystallisation and encourage grain growth, shown to improve the properties of Fe-6.5 wt%Si built by AM [26]. The component was left attached to the baseplate during heat treatment to allow a flatness tolerance of 0.03 mm for the lower face, and a parallel tolerance of 0.03 mm for the upper face, to be achieved upon removal of the component using EDM. If the removal of the component was completed before heat treatment, there were concerns that the part may distort and be unable to achieve the required tolerance.

Images of the stator are shown in Fig. 6 demonstrating the successful resolution of the tooth profile. It has not yet been possible to check the cross-sectional profile of the back iron as sectioning and polishing would render it unusable. Following EDM removal from the baseplate, the component shows oxidisation throughout due to the sensitive nature of this alloy and the contact with water during the EDM process. The oxidisation is not suspected to have a significant impact on the performance of the component, however in the future methods to prevent this such as coating before EDM could be implemented by dipping the component, whilst allowing the baseplate and bottom 0.5 mm clear of insulation to allow for EDM. The lower surface could then be coated following EDM. EDM could also be performed in oil instead of water circumventing the issue, then coated. The stator mass is 0.66 kg, giving a stacking factor of 65–70%. The original electrical steel lamination stator has a mass of 0.97 kg with a stacking factor of approximately 91%. A comparison of time and cost to manufacture both prototype stators are shown in Table 1. The processing cost for the AM stator includes machine time ($1200), heat treatment ($350), and EDM removal ($100), whereas for the laminations this includes winding, bonding, welding, milling, and insulating.

Table 1
Time and cost of manufacturing Hilbert AM and 0.127 mm electrical steel lamination.

	Raw material ($)	Processing cost ($)	Processing time (weeks)
Hilbert AM	40	1650	3
0.127 mm Laminations	20	2500	12
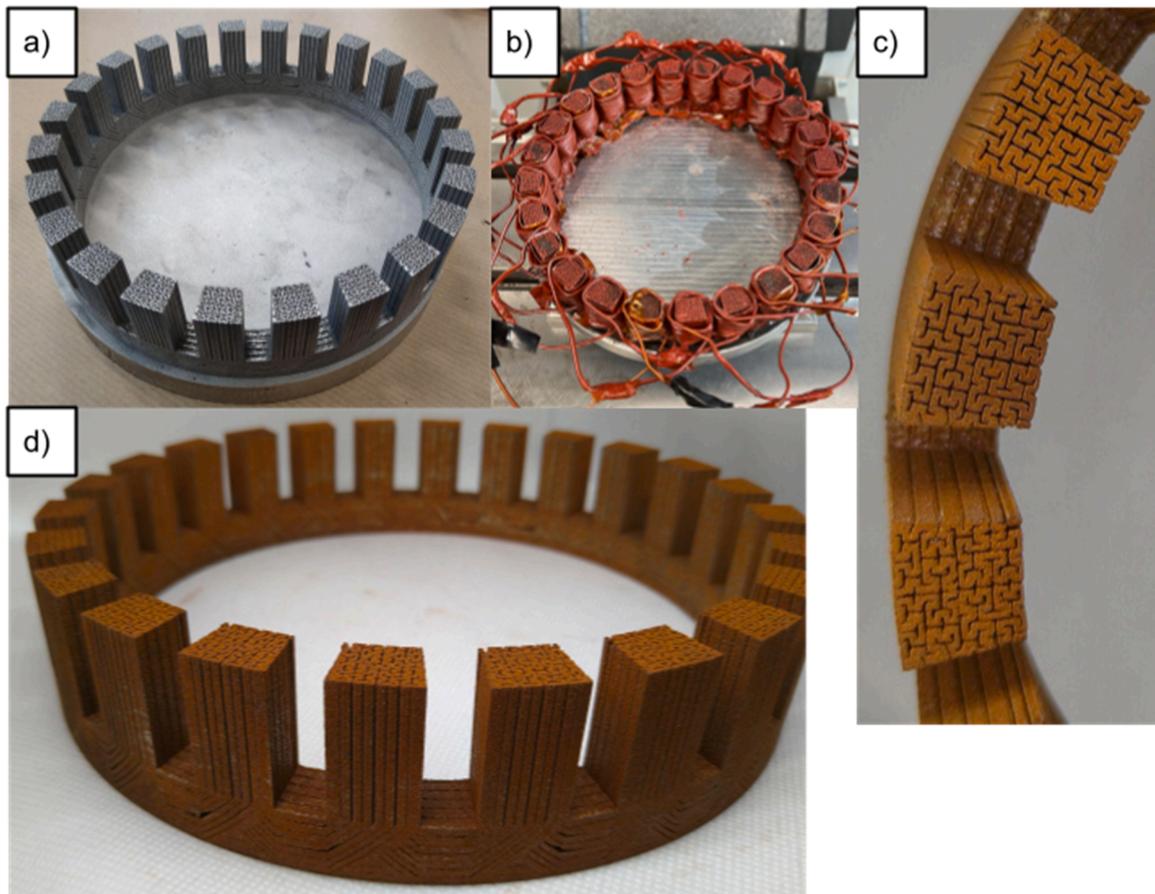
Fig. 6. Images of the Hilbert stator showing the as-built component still attached to the build plate (a), the part after removal from the build plate (d), and the successfully resolved tooth profile (c), both showing severe oxidisation. The stator is also shown in the wound state ready for rig testing (b).

3.3. Characterisation of Hilbert AM stator

A no-load test and a static test were performed to measure stator iron losses and the torque capability of the machine respectively. Details of the static test procedure and test setup can be found in [28]. The AM Hilbert stator was experimentally tested and compared with a 0.127 mm lamination stator, and the core loss behaviour was also calculated using FEA for both a 0.127 mm lamination and a 0.35 mm lamination. The static torque curves are shown in Fig. 7a, normalised to the rated torque of 18 Nm and rated current of 140 A. The AM Hilbert stator shows a decrease in torque throughout the full range of tested values, with a 17% decrease at 20 A (14% of rated current) through to a 23% decrease at 140 A. This trend shows a higher difference between the laminations and AM Hilbert stators with increasing current. This is unsurprising considering the mass difference between the two stators, with less material giving a lower magnetic flux in the machine. Gravimetric torque density was calculated at 100% of the rated current (140 A) for the stator only, showing 18.3 Nm/kg for the 0.127 mm lamination stator and 20.7 Nm/kg for the AM Hilbert stator.

The core loss behaviour of two experimentally tested stators is displayed in Fig. 7b along with the FEA results from laminations of two different thicknesses. The FEA of the 0.127 mm lamination shows a good correlation with the experimental data for 0.127 mm laminations, displaying that the FEA model is successful in its loss predictions. FEA data for a 0.35 mm lamination stator was also created. The AM Hilbert stator shows higher core loss than all the other samples at higher frequencies above 500 Hz, with the core loss at 800 Hz being 543 W, 27% higher than the 0.35 mm laminations and 210% higher than those of the 0.127 mm laminations. At lower frequencies, the performance of the AM Hilbert stator is comparable to both the 0.127 mm and 0.35 mm laminations.

4. Discussion

Resolving the Hilbert cross-sectional pattern is difficult in the XZ plane of the machine as the laser melts through multiple layers for each hatch, enabling a 3D component to be created. However, when trying to resolve cross-sections that have gaps where no material should be, the laser burns through and melts powder which should not be melted. In this study we created a design rule to allow this to be managed through the design of the component however other strategies are available. Different parameters can be used for the upskin surfaces to reduce the laser power or increase the speed, giving a shallower melt pool and hence less burn-through. Optimisation studies into this method could yield further improvements in the minimum gap distance and hence increase the stacking factor of these components. Another possible

improvement to the cross-sectional resolution and prevention of short-circuiting could be in post-processing the components using a chemical or electro-polishing process. This would preferentially remove material from things like partially melted particles or thin sections due to their high surface area to volume ratio, enabling the reduction of undesirable short circuits from the component. Other methods to do this could be abrasive flow machining (AFM) if the cross-section had a closed shape or by using a fixture for this. As a secondary benefit from this, it is possible that a component with a smoothed surface could demonstrate softer magnetic performance as the rough surfaces may act as pinning sites for magnetic domains. In this study, some cracking was evident in the Hilbert section in Fig. 2c which could also impact the magnetic performance.

Other cross-sectional geometries may offer an improvement over the Hilbert space-filling curve design. Hilbert geometry has been shown to provide an improvement over other sections such as a lamination style design [16], however, with AM there is an enormous design space to explore. Multi-physics simulations including the magnetic performance and loss behaviour are computationally expensive for these geometrically complex components. Further to this, these simulations must be completed in 3D as any magnetic circuit in 2D would currently perform better with laminations. The simulation of the Hilbert stator used in this study was attempted but not possible to solve based on computational demands. The Hilbert geometry has many overhanging horizontal surfaces which are known to be difficult to process via AM. Other geometries may be more friendly to the AM process whereby overhanging surfaces are limited to below angles of approximately 45°. To obtain the optimal geometry for a given machine, new software capable of topology optimisation based on magnetic performance would be required, whilst respecting manufacturing constraints. This would allow the best shape to be obtained for a given application, in the same way as structural parts are intelligently optimised with topology optimisation currently.

The geometry of the final component depends not only on the CAD file but also on the processing parameters such as hatch spacing, melt pool width, and hatch offsets from the edge of the part. All of these parameters can influence the position of the component's surface in relation to the CAD surface. Hence, optimisation of these parameters could also reduce the minimum gap required to ensure electrical isolation.

The stator in this study suffered from corrosion, and although it was judged that this wouldn't have a significant impact on the magnetic performance of the component in characterisation tests, it would be unlikely to be acceptable in the manufacture of an electrical machine for use in an application as the oxidisation could deteriorate with time. It would be possible to prevent this by either potting the stator as per
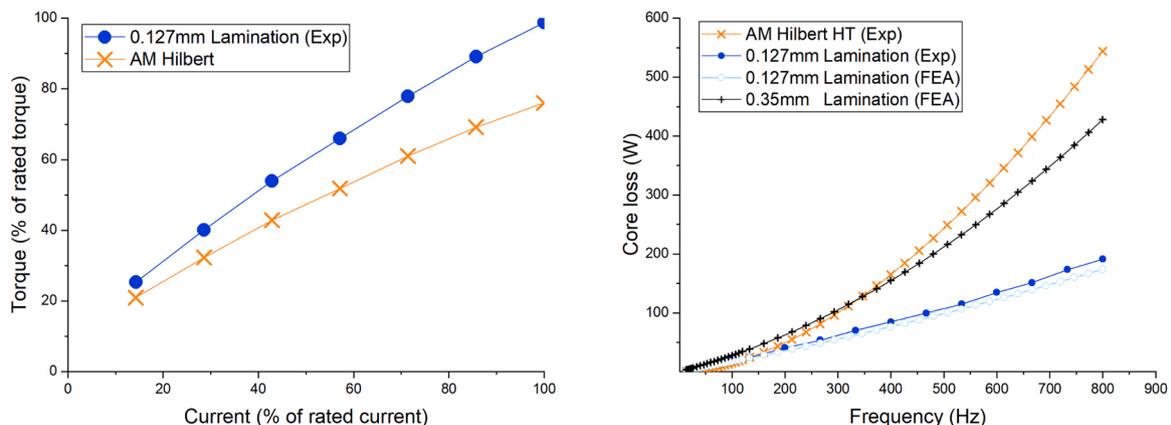
Fig. 7. Torque performance of AM Hilbert stator and 0.127 mm laminations stator (a), demonstrating a reduction in torque of approximately 20% throughout the whole operating range. Loss performance (b) measured at several frequencies shows that the AM Hilbert stator has higher core loss than the 0.127 mm laminations, but is comparable to 0.35 mm laminations through a range of frequencies.

traditional electrical machine manufacturing processes or infiltrating it with some kind of surface coating before EDM removal from the baseplate.

The reduction in torque when using the AM Hilbert stator can be expected as there is a lower volume of magnetic material when compared to the laminated stator. However, the gravimetric torque density of 20.7 Nm/kg for the AM Hilbert stator, which is 13% higher than that of the 0.127 mm laminated component, shows the AM Hilbert stator outperforming that of the laminated stator for the same mass. To allow for the same torque it would be possible to increase the cross-sectional area of the tooth of the stator, whilst reducing the area of the slot and therefore being able to manage the low stacking factor. By using AM to also create the copper windings the same amount of conductive material could be used even with a smaller slot, whilst increasing the amount of soft-magnetic material in the core within the same volumetric envelope. An example of these windings were created (Fig. 8), showing that the slot fill factor could be doubled, as it was possible to create windings with a cross-sectional area of 2.4 × 2.7 mm with AM, whereas due to winding constraints, the original machine used conductors with a cross-section area of 1.2 × 2.7 mm. By reducing the slot size and increasing the tooth area, it would be possible to maintain the same level of torque.

The core loss of the AM Hilbert stator was higher than that of the laminations, reaffirming that if a 2D magnetic circuit is needed then laminations are still the preferred method. The core loss is close to that of the thicker lamination showing promise for enabling electrical machines with 3D flux paths. The 0.127 mm laminated stator shown in this study had a large cost due to it being a low-volume prototype, however, many issues were found with the manufacturing of this component making it unsuitable for volume production. Winding and bonding the laminations is a difficult process and machining the slots after this can cause issues with delamination and show areas of insufficient bonding (Fig. 9). If this component were possible to mass manufacture, the cost would likely be significantly lower than the AM component. The AM component was also manufactured more quickly in only a few weeks, compared to the 12-week lead time for the prototype laminated stator. This can enable a larger design space to be explored in the same amount of time, allowing electrical engineers greater freedom to manipulate the architecture of the machine. The AM stator also had some build defects (Fig. 9). For prototypes this is likely to be an acceptable compromise, however for production components improvements would be required in the build to reduce or eliminate these defects.

The core loss of this part was measured with a heat-treated sample which is likely to have recrystallized and experienced grain growth, similar to the components reported by Garibaldi et al. [26]. Grain growth up to a size of 5–7 mm has been shown to improve properties at a frequency of 50–60 Hz, however, smaller grain size has been shown to

have reduced losses at high frequencies [31]. Therefore, the as-built condition with its smaller grain size of 10–100 μm may have lower losses at higher frequencies. A sample was built to investigate this, however, it was unfortunately broken during transit.

Build time was quite large at 80 h due to the complex scanning pattern required. A large area in the centre of the build does not have any material, meaning lots of time is spent with the laser traversing this region without melting any material. It was possible to reduce this to approximately 25 h by splitting the component into quarters, however, this can create a weld line and it is not known the effect that this may have on the magnetic properties of the component. The component that broke in transit was suspected to fail because of these weld lines. The joints were orientated vertically, meaning that any faults between the segments were stacked on top of each other. In further work, this split should be angled to allow the penetration of multiple layers by the laser, to bridge the gap between the segments and create a better joint. The impact on the magnetic properties of these joins should also be investigated.

This study, to the author's knowledge, is the first use of 3D magnetic flux paths in an electrical machine stator made with eddy current limiting geometry. This technology can enable different architectures of electrical machine that require 3D flux paths, which has previously not been possible. Hence, there has been little development of motors of this type, however, some examples could be conical motors with magnetically levitating bearings [7,8], or any motor where SMC has previously been used. By using AM to process the functional materials required for electrical machines, the limitations are now in the mind of the designer, and it is possible to realise architectures never before possible.

A demonstrator motor was created to showcase the possibilities of using AM for electrical machine design (Fig. 10). The housing can be made from lightweight material and have additional functionality built into it such as heat exchangers. The stator can be spatially graded to have different structures depending on the flux pathway or direction, and can possibility incorporate air or liquid cooling when using cross-sectional geometries such as the Hilbert pattern. Conductive coils can have spatially varied cross-sectional area [31] to reduce losses, have better slot fill factors due to pre-shaping and also have higher temperature insulators as there is little need to deform the part and hence brittle ceramics can be used to insulate conductors for the first time.

5. Conclusion

Toroidal ring samples were built using AM from high silicon electrical steel powder (Fe-6.5 wt%), with a Hilbert cross-sectional geometry implemented to reduce eddy current losses during AC excitation. Heat treatment was found to improve the properties of these toroidal rings by increasing permeability and reducing core losses, 'squaring' the

Fig. 8. Increasing the slot fill factor is demonstrated using L-PBF of pure copper, doubling the slot fill factor.
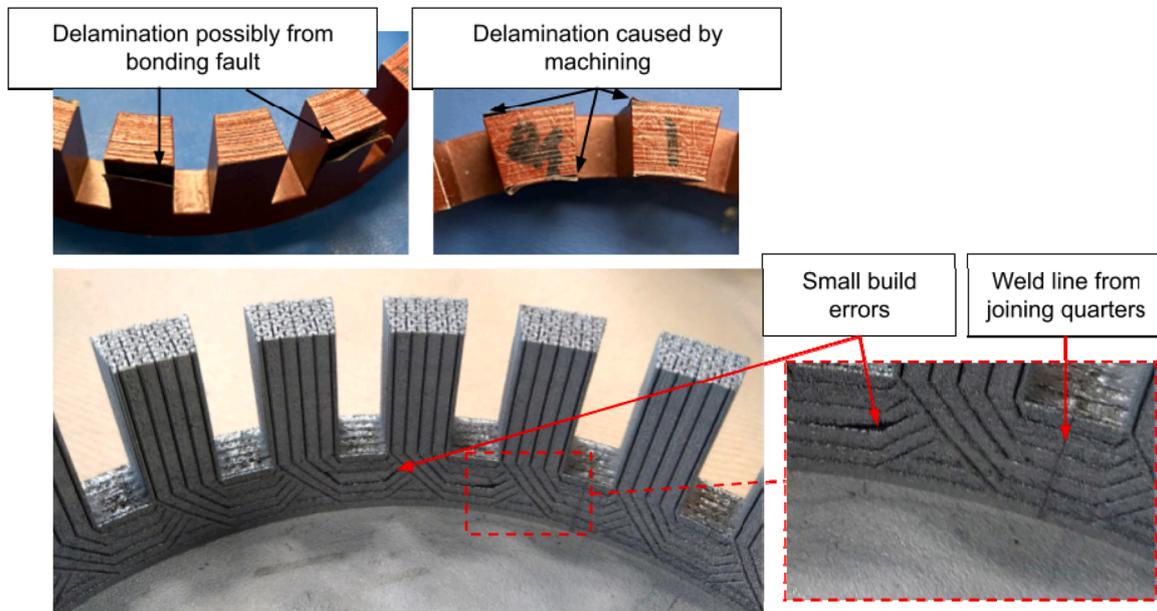
Fig. 9. Delamination from bonding and machining showed for the 0.127 mm laminated stator, and build defects of the AM Hilbert stator showing a weld line from splitting the component into four segments, and small errors where the geometry is not exactly as intended.
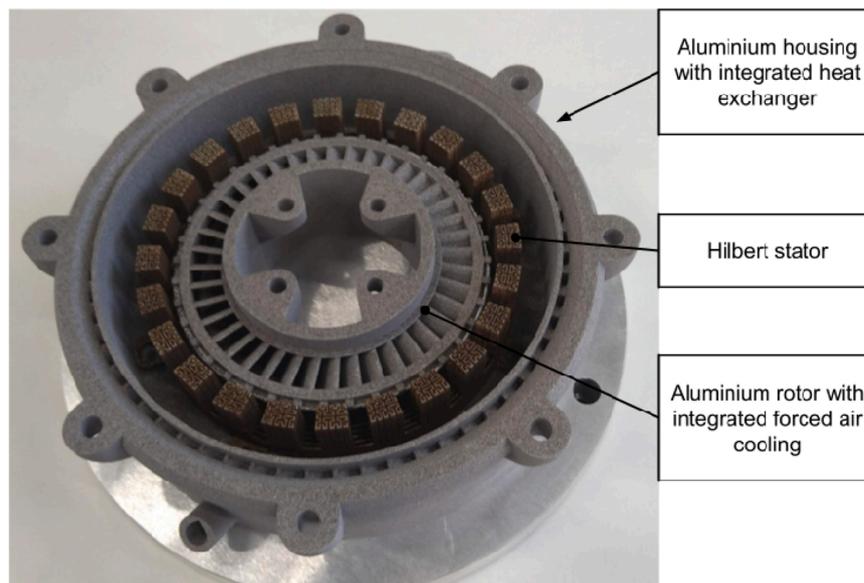
Fig. 10. Demonstrator motor created mostly with AM, showing a soft magnetic FeSi stator core and rotor back iron, an aluminium housing and rotor. The bearings and permanent magnets are not created using AM.

BH loop. This Hilbert cross-sectional geometry was then implemented into the 3D magnetic flux pathways of an axial flux permanent magnet electrical machine, which was compared experimentally to 0.127 mm thickness electrical steel laminations (Fe-3 wt%Si) and by using FEA with 0.35 mm thick electrical steel laminations (Fe-3 wt%Si). The AM Hilbert stator was 34% lighter than the 0.127 mm laminations and showed an average of 20% reduction in torque throughout the operating range. The torque density of the AM Hilbert stator was 13% higher at 20.7 Nm/kg (stator only) than the 0.127 mm laminations. Core losses in the AM Hilbert stator were higher than the 0.127 mm laminations, but comparable to 0.35 mm laminations for frequencies below 500 Hz. At 1000 Hz the experimental core loss of the AM Hilbert stator was 543 W, compared to 428 W for the 0.35 mm laminations calculated using FEA. To the authors knowledge, this is the first time an additively manufactured soft-magnetic component has been directly compared to electrical

steel laminations in an application using 3D magnetic flux pathways. Improvements in the AM Hilbert stator could have been obtained by reducing the undesired electrical shorting between areas of material that should be electrically isolated, and by improving AM build parameters to reduce the size of insulating air gaps, hence increasing the stacking factor. Future work will address the loss of torque due to the reduction of total magnetic material, and offsetting this by increasing the area of the stator tooth, whilst reducing the size of the slots. The same amount of conductive material could be used by utilising AM to manufacture the windings, allowing the full torque to be obtained.

CRediT authorship contribution statement

Alexander D. Goodall: Conceptualization, Data curation, Formal analysis, Investigation, Methodology, Writing – original draft. **FNU**

Nishanth: Data curation, Formal analysis, Methodology, Investigation, Writing – review & editing. **Eric L. Severson:** Methodology, Supervision, Writing – review & editing. **Iain Todd:** Conceptualization, Data curation, Formal analysis, Methodology, Funding acquisition, Supervision, Visualisation, Writing – review & editing.

Declaration of Competing Interest

The authors declare that they have no known competing financial interests or personal relationships that could have appeared to influence the work reported in this paper.

Data availability

Data is shared in the article.

Acknowledgements

References

[1] P. Beckley, Electrical Steels for Rotating Machines, IET, 2002.

[2] A. Schoppa, P. Delarbre, Soft magnetic powder composites and potential applications in modern electric machines and devices, IEEE Trans. Magn. 50 (2014) 1–4, https://doi.org/10.1109/TMAG.2013.2290135.

[3] F. Nishanth, J.V. Verdeghem, E.L. Severson, Recent Advances in Analysis and Design of Axial Flux Permanent Magnet Electric Machines, in: 2021 IEEE Energy Convers. Congr. Expo. ECCE, 2021: pp. 3745–3752. https://doi.org/10.1109/ECCE47101.2021.9595085.

[4] M. Liben, D.C. Ludois, Analytical Design and Experimental Testing of a Self-Cooled, Toroidally Wound Ring Motor With Integrated Propeller for Electric Rotorcraft, IEEE Trans. Ind. Appl. 57 (2021) 2342–2353, https://doi.org/10.1109/TIA.2021.3058197.

[5] Design, modelling and optimisation of a slot-less axial flux permanent magnet generator for direct-drive wind turbine application - Ghaheri - 2020 - IET Electric Power Applications - Wiley Online Library, n.d. ⟨https://ietresearch.onlinelibrary.wiley.com/doi/full/10.1049/iet-epa.2019.0385⟩ (accessed March 31, 2023).

[6] F. Sahin, Design and development of a high-speed axial-flux permanent-magnet machine. Phd Thesis 1 (Research TU/e / Graduation TU/e), Technische Universiteit Eindhoven, 2001, https://doi.org/10.6100/IR544267.

[7] P. Kascak, R. Jansen, T. Dever, A. Nagorny, Dr.K. Loparo, Bearingless five-axis rotor levitation with two pole pair separated conical motors, 2009 IEEE Ind. Appl. Soc. Annu. Meet. (2009) 1–9, https://doi.org/10.1109/IAS.2009.5324866.

[8] G. Messager, A. Binder, Derivation of forces and force interferences in a double conical high-speed bearingless permanent magnet synchronous motor, in: 2017 IEEE Int. Electr. Mach. Drives Conf. IEMDC, 2017: pp. 1–8. https://doi.org/10.1109/IEMDC.2017.8002213.

[9] Y. Wang, J. Lu, C. Liu, G. Lei, Y. Guo, J. Zhu, Development of a High-Performance Axial Flux PM Machine With SMC Cores for Electric Vehicle Application, IEEE Trans. Magn. 55 (2019) 1–4, https://doi.org/10.1109/TMAG.2019.2914493.

[10] S. Sun, F. Jiang, T. Li, B. Xu, K. Yang, Comparison of a multi-stage axial flux permanent magnet machine with different stator core materials, IEEE Trans. Appl. Supercond. 30 (2020) 1–6, https://doi.org/10.1109/TASC.2020.2990761.

[11] C.-W. Kim, G.-H. Jang, J.-M. Kim, J.-H. Ahn, C.-H. Baek, J.-Y. Choi, Comparison of axial flux permanent magnet synchronous machines with electrical steel core and soft magnetic composite core, IEEE Trans. Magn. 53 (2017) 1–4, https://doi.org/10.1109/TMAG.2017.2701792.

[12] G. Ouyang, X. Chen, Y. Liang, C. Macziewski, J. Cui, Review of Fe-6.5 wt%Si high silicon steel—A promising soft magnetic material for sub-kHz, Appl., J. Magn. Magn. Mater. 481 (2019) 234–250, https://doi.org/10.1016/j.jmmm.2019.02.089.

[13] G. Tian, X. Bi, Study on the Si penetration into Fe sheets using PVD method and its application in the fabrication of Fe-6.5wt% Si alloys, Surf. Coat. Technol. 204 (2010) 1295–1298, https://doi.org/10.1016/j.surfcoat.2009.10.014.

[14] A. Krings, M. Cossale, A. Tenconi, J. Soulard, A. Cavagnino, A. Boglietti, Magnetic materials used in electrical machines: a comparison and selection guide for early machine design, IEEE Ind. Appl. Mag. 23 (2017) 21–28, https://doi.org/10.1109/MIAS.2016.2600721.

[15] M. Garibaldi, I. Ashcroft, M. Simonelli, R. Hague, Metallurgy of high-silicon steel parts produced using Selective Laser Melting, Acta Mater. 110 (2016) 207–216, https://doi.org/10.1016/j.actamat.2016.03.037.

[16] A. Plotkowski, J. Pries, F. List, P. Nandwana, B. Stump, K. Carver, R.R. Dehoff, Influence of scan pattern and geometry on the microstructure and soft-magnetic performance of additively manufactured Fe-Si, Addit. Manuf. 29 (2019), 100781, https://doi.org/10.1016/j.addma.2019.100781.

[17] D. Goll, J. Schurr, F. Trauter, J. Schanz, T. Bernthaler, H. Riegel, G. Schneider, Additive manufacturing of soft and hard magnetic materials, Procedia CIRP 94 (2020) 248–253, https://doi.org/10.1016/j.procir.2020.09.047.

[18] D. Goll, D. Schuller, G. Martinek, T. Kunert, J. Schurr, C. Sinz, T. Schubert, T. Bernthaler, H. Riegel, G. Schneider, Additive manufacturing of soft magnetic materials and components, Addit. Manuf. 27 (2019) 428–439, https://doi.org/10.1016/j.addma.2019.02.021.

[19] B. Koo, M.-S. Jang, Y.G. Nam, S. Yang, J. Yu, Y.H. Park, J.W. Jeong, Structurally-layered soft magnetic Fe-Si components with surface insulation prepared by shell-shaping selective laser melting, Appl. Surf. Sci. 553 (2021), 149510, https://doi.org/10.1016/j.apsusc.2021.149510.

[20] A. Andreiev, K.-P. Hoyer, D. Dula, F. Hengsbach, M. Haase, J. Gierse, D. Zimmer, T. Tröster, M. Schaper, Soft-magnetic behavior of laser beam melted FeSi3 alloy with graded cross-section, J. Mater. Process. Technol. 296 (2021) 117183, https://doi.org/10.1016/j.jmatprotec.2021.117183.

[21] H. Tiismus, A. Kallaste, A. Belahcen, M. Tarraste, T. Vaimann, A. Rassõlkin, B. Asad, P. Shams Ghahfarokhi, AC Magnetic Loss Reduction of SLM Processed Fe-Si for Additive Manufacturing of Electrical Machines, Energies 14 (2021) 1241, https://doi.org/10.3390/en14051241.

[22] A. Manninen, J. Pippuri-Mäkeläinen, T. Riipinen, T. Lindroos, S. Metsä-Kortelainen, A. Antikainen, The Mitigation of Eddy-Current Losses in Ferromagnetic Samples Produced by Laser Powder Bed Fusion, IEEE Access 10 (2022) 115571–115582, https://doi.org/10.1109/ACCESS.2022.3218669.

[23] N. Urban, M. Masuch, J. Paduch, J. Franke, An Approach to Eddy Current Reduction in Laser Powder Bed Fused High Silicon Steel Considering Manufacturing Influences, in: 2021 11th Int. Electr. Drives Prod. Conf. EDPC, 2021: pp. 1–5. https://doi.org/10.1109/EDPC53547.2021.9684214.

[24] T. Pham, P. Kwon, S. Foster, Additive manufacturing and topology optimization of magnetic materials for electrical machines—a review, Energies 14 (2021) 283, https://doi.org/10.3390/en14020283.

[25] A. Plotkowski, K. Carver, F. List, J. Pries, Z. Li, A.M. Rossy, D. Leonard, Design and performance of an additively manufactured high-Si transformer core, Mater. Des. 194 (2020), 108894, https://doi.org/10.1016/j.matdes.2020.108894.

[26] M. Garibaldi, I. Ashcroft, J.N. Lemke, M. Simonelli, R. Hague, Effect of annealing on the microstructure and magnetic properties of soft magnetic Fe-Si produced via laser additive manufacturing, Scr. Mater. 142 (2018) 121–125, https://doi.org/10.1016/j.scriptamat.2017.08.042.

[27] BSI, BS60404–6-2018 Methods of measurement of the magnetic properties of magnetically soft metallic and powder materials at frequencies in the range 20 Hz to 100 kHz by the use of ring specimens, 2018.

[28] F. Nishanth, G. Bohach, M.M. Nahin, J. Van de Ven, E.L. Severson, Development of an Integrated Electro-Hydraulic Machine to Electrify Off-highway Vehicles, IEEE Trans. Ind. Appl. (2022) 1–12, https://doi.org/10.1109/TIA.2022.3189609.

[29] Simcenter MAGNET | Siemens Software, Siemens Digit. Ind. Softw., n.d. ⟨https://www.plm.automation.siemens.com/global/en/products/simcenter/magnet.html⟩ (accessed November 27, 2022).

[30] M.H. Rashid, Power Electronics Handbook, Butterworth-Heinemann,, 2017.

[31] N. Simpson, S.P. Munagala, A. Catania, F. Derguti, P.H. Mellor, Functionally Graded Electrical Windings Enabled by Additive Manufacturing, in: 2022 Int. Conf. Electr. Mach. ICEM, 2022: pp. 1477–1483. https://doi.org/10.1109/ICEM51905.2022.9910912.